Methodology Article

Design and Simulation of an Ultrahigh-resolution Spectral-domain Optical Coherence Tomography

Mohammad Hossein Vafaie, Maryam Ansarian, Hossein Rabbani

Medical Image and Signal Processing Research Center, School of Advanced Technologies in Medicine, Isfahan University of Medical Sciences, Isfahan, Iran

Abstract

Background: Optical coherence tomography (OCT) is a biomedical imaging technique used to achieve high-resolution images from human tissues in a noninvasive manner. **Methods:** In this article, a practical approach is proposed for designing ultrahigh-resolution spectral-domain OCT (UHR SD-OCT) devices. At first, block diagram of a typical SD-OCT is introduced in detail. At second, internal components of each arm are introduced where the key parameters of each component are highlighted. At third, the effects of these key parameters on the overall performance of the UHR SD-OCT are investigated in a comprehensive manner. At fourth, the most important requirements of a UHR SD-OCT are explained, where suitable optical equipment is selected for each arm based on these requirements. At fifth, optical accessories as well as the electrical devices required for managing and control of the performance of a UHR SD-OCT are introduced in brief. **Results:** Performance of the proposed device is assessed through various simulations, and finally, the implementation cost and implementation challenges are investigated in detail. **Conclusions:** Simulation results indicate that the proposed UHR SD-OCT has acceptable axial resolution and imaging depth; hence, it is a good candidate for use in retinal applications that require UHR imaging.

Keywords: *Imaging devices, optical coherence tomography, spectral domain optical coherence tomography*

Submitted: 22-May-2024 **Revised:** 14-Oct-2024 **Accepted:** 15-Oct-2024 **Published:** 19-Apr-2025

Introduction

Optical coherence tomography (OCT) is a biomedical imaging technique used to achieve high-resolution two-dimensional (2-D) and three-dimensional (3-D) images from human tissues in a noncontact noninvasive manner. One of the most popular usages of OCT devices is in retinal imaging.[1,2]

The basics of OCT imaging are almost similar to ultrasound imaging with one difference that in OCT a broadband light source is used for image construction instead of an acoustic source. As a result, due to higher travel speed of a light ray in comparison with a sound, it is not possible to measure the travel time of the radiated light ray through common measurement tools.[3] Therefore, special optical elements must be adopted in OCTs to extract the information and construct the image.

In OCTs, the light ray produced by the light source is divided into two parts: the first part is transferred to the reference arm while the second part is transferred to the sample arm. The light ray transferred to the reference arm hits the reference mirror and returns back while the light ray transferred to the sample arm penetrates into the sample tissue and returns back.[4] Both the returned light rays interfere with each other where the resultant light ray is transferred to a detector for image construction.

To achieve a proper interference, returning light rays from both the sample and reference arms must reach the fiber coupler in a same time. Since travel speed of the light in both the arms is the same, to satisfy the constrained, above, it is essential that both the sample and reference arms have the same length.[5]

In the first generation of OCTs, referred to time domain-OCT (TD-OCT),[6] the reference mirror is moved quickly to scan the preferred depth of the sample tissue.

How to cite this article: Vafaie MH, Ansarian M, Rabbani H. Design and simulation of an ultrahigh-resolution spectral-domain optical coherence tomography. J Med Signals Sens 2025;15:12.

Address for correspondence:
Dr. Mohammad Hossein Vafaie, Medical Image and Signal Processing Research Center, School of Advanced Technologies in Medicine, Isfahan University of Medical Sciences, Isfahan, Iran.
E-mail: mh.vafaie@amt.mui.ac.ir

Access this article online

Website: www.jmssjournal.net

DOI: 10.4103/jmss.jmss_36_24

Quick Response Code:

Due to limitations in mechanical movement of the reference mirror, the resultant scan rate of TD-OCTs is below the minimum requirement of high-performance applications.[7]

To overcome this shortcoming, the second generation of OCTs, referred to Fourier domain-OCT (FD-OCT), is proposed in which no movable mirror is required. In FD-OCTs, a special light source as well as a high-resolution spectrometer arm is adopted to extract the depth information of the sample tissue.[8] So far, FD-OCTs are categorized in two types: spectral domain-OCTs (SD-OCTs) and swept source-OCTs (SS-OCTs).

In SD-OCT, a light source with high bandwidth is adopted to achieve the required axial resolution. Moreover, output beam of the light source is transferred to a fiber coupler that divides the light beam into two parts. Similar to TD-OCTs, the first part is transferred to the reference arm and the second part is transferred to the sample arm. Then, the returned light rays interfere with each other where the obtained light ray is transferred to the spectrometer arm. In the spectrometer arm, the light ray is decomposed into its constituent light rays which are focused on a line-scan camera pixel array. Finally, the digital output of the camera is transferred to a personal computer (PC) where several processing algorithms such as noise cancellation, common mode term rejection, moving average filtration, and inverse fast Fourier Transformation $^{-1}$ are applied to construct the images.[9,10]

In SS-OCTs, a narrow bandwidth laser is used as a light source where the central wavelength of the laser source is swept very quickly; that is, in SS-OCTs, instead of using a movable reference mirror, a laser source with variable central wavelength is adopted.[11] Performance of SS-OCTs is just similar to SD-OCTs with this difference that instead of a spectrometer arm, a detector array is used in SS-OCTs to construct the images. To do this, the light beam generated after interference is applied to a detector array, and then, the voltage sensed by each detector is converted to a digital value using a fast data acquisition (DAQ) card.[12] The generated digital values are used to construct the OCT image.[13]

According to the structure of SD-OCT and SS-OCT, pros and cons of each type can be summarized as follows:

(1) In SS-OCT, narrow bandwidth, high speed, frequency swept-able laser sources are necessary for image construction which increases the implementation cost significantly[14]
(2) In SD-OCT, a line-scan camera is necessary in spectrometer arm which degrades the A-scan rate. Therefore, A-scan rate of SD-OCTs is significantly lower than that of SS-OCTs[15]
(3) In SD-OCT, a broadband light source as well as a high-resolution spectrometer arm must be used for image construction; hence, axial resolution and phase stability of SD-OCT are considerably higher than that of SS-OCT
(4) In SS-OCT, images are constructed by adopting a detector array as well as a DAQ card. However, in spectrometer arm of a SD-OCT, complex optical elements must be used to obtain image information. As a result, design, implementation, and performance evaluation of SD-OCTs are more complex; hence, the main topic of this study is dedicated to feasibility study of ultrahigh-resolution SD-OCT (UHR SD-OCT) design.

In recent decades, SD-OCT becomes a widely popular imaging technology used in many clinical applications. Despite such fast growth, the technology behind constructing these devices has been limited to some countries and not been readily accessible to many researchers due to the cost of the commercially available devices and lack of essential knowledge in the field of optics. To overcome this shortcoming, mentioned above, this article aims to provide a detailed procedure on the design of a custom UHR SD-OCT device. The effects of multiple design parameters on the overall performance of the imaging system are analyzed while discussions are provided to serve as a guideline for the development of a SD-OCT system. While this article can be generalized for different applications, the article focuses on the design of a SD-OCT system that can be used in retinal applications. Based on a study by Chinn *et al*.,[14] the resolution of available commercial SD-OCTs is not sufficiently high to predict the diabetic diseases from the obtained images; that is, by increasing the resolution of the SD-OCT images the probability of early-stage detection of diabetic diseases can be increased effectively. Therefore, this article focuses on the design procedure of a UHR SD-OCT that can be used in retinal applications. The article explains procedures to measure the axial and lateral resolutions and field of view (FOV) of the system and to understand the trade-off between optical specifications of a typical SD-OCT.

The organization of this article is as follows: in Section II, internal structure of SD-OCT is presented, whereas in Section III, the procedure of optical system design is presented. In Section IV, a UHR SD-OCT is designed and its optical elements are selected. Simulation results are presented in Section V and conclusions are presented in Section VI.

User Requirements and Risk Analysis

User requirements

User requirements are the fundamental requirements affect the development of any medical device. After assessing recent traditional SD-OCTs and conducting several meetings with expert ophthalmologist, fundamental requirements of the desired UHR SD-OCT that can be used in retinal application are identified carefully and are tabulated in Table 1. Design and development of the UHR SD-OCT must be conducted such that all of the user requirements are satisfied.

Risk analysis

Risk analysis is another fundamental issue that affects the development of any medical device. After conducting

several meetings with expert ophthalmologist, the following three issues are the most common risks evident in the OCTs:

(i) Damage to the patient retina due to impermissible radiation time or intensity

(ii) Incorrect scanning of the cross-section of the patient retina due to improper control of the galvanometric mirrors

(iii) Improper extraction of A-scans from the raw A-scans due to improper execution of digital signal algorithms. Design and development of the UHR SD-OCT must be conducted such that all of the risks, above, are mitigated.

Internal Structure of Spectral Domain-optical Coherence Tomography

System requirements

In the following paragraphs, optical components of the proposed UHR SD-OCT are introduced according to the user requirements and risk analysis mentioned in Section II. After that, each component is designed in a way that it addresses one or more system requirements or mitigates one or more risks.

Light source and its accessories

Block diagram of a SD-OCT as well as its optical equipment is illustrated in Figure 1. As mentioned earlier, a low-coherence light source must be used in SD-OCTs to achieve high-resolution images.

Often in SD-OCTs, a super luminescent diode (SLD) is used as a light source. The power spectral distribution of the SLD has significant effects on the overall performance of SD-OCT. Based on Ishida *et al.,* and Braaf *et al.,*[16,17] Gaussian distribution is the best distribution for the SLD light sources used in SD-OCTs.

Often, a small portion of the light transferred to the arms is returned back to the light source. This returning ray can damage the light source; hence, an optical isolator is placed after the light source. Optical isolator provides a unidirectional path for the light; that is, the light entered into the isolator can travel without any significant attenuation while the returning light ray is attenuated significantly.[18]

A fiber coupler is placed after the optical isolator to divide the light into two parts. Fiber coupler performs the following two tasks:

(1) Divides the light into two parts with adjustable intensities while the wavelength specifications of both the parts are just similar to the main light. The light rays returned back from the sample and reference arms interfere in the coupler

(2) Transmits the light generated from the interference to the spectrometer.[19]

Fiber couplers are accessible with different power ratios where the best option is selected based on the intensity of the light source and the OCT application.[20]

Sample arm

Lateral resolution and maximum FOV of SD-OCT depend on the optical elements used in the sample arm.[21,22] Graphical representation of lateral resolution, depth of focus (DOF), and FOV is illustrated in Figure 2.

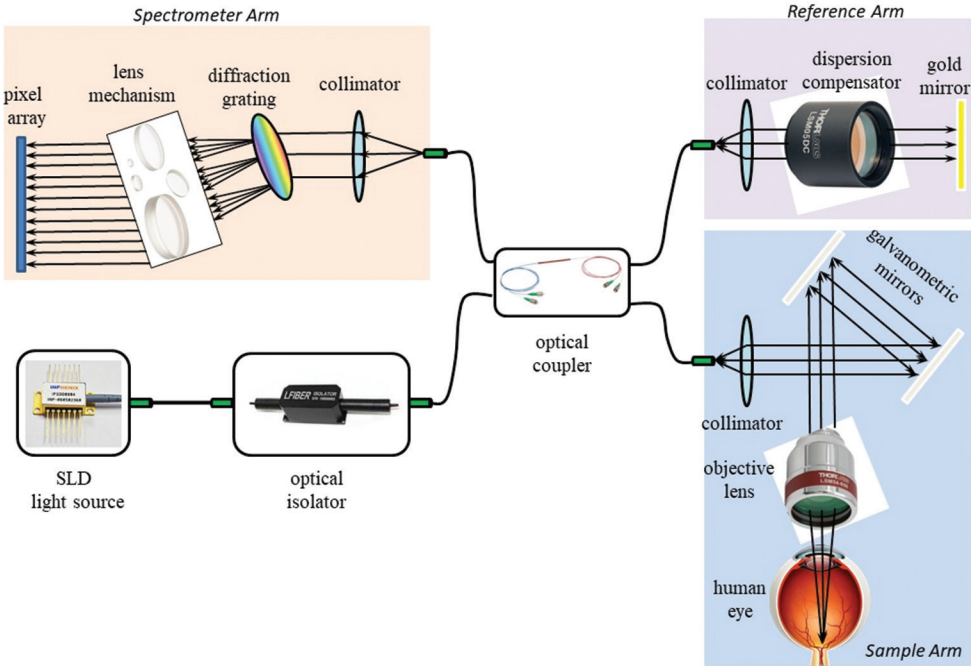

Figure 1: Block diagram of a typical spectral domain-optical coherence tomography. SLD: Super luminescent diode

Based on Figure 1, sample arm of a SD-OCT consists of the following components:

- Collimator
- Galvanometric mirrors
- Objective lens.

In the following paragraphs, a brief description is provided about these components.

Collimator: Collimators usually consist of one or more lenses. Collimators must be placed in the entrance of all the SD-OCT arms to connect the optical fiber with FC/APC connector to the arms.[23]

Collimator performs the following two tasks in the sample arm:

(i) Parallelizes the light ray entered into the arm to produce a light ray with specified diameter. Diameter of this parallelized light depends on the collimator specifications. The parallelized light ray travels in the sample arm, penetrates into the sample, and returned back to the collimator

(ii) Focuses the light ray travels back from the sample tissue to the central point of the optical fiber.

Collimator must be designed and fabricated such that the entrance of the sample arm exactly coincides with the focal point of the collimator lenses. Since satisfying this constraint is tedious and requires special equipment, collimators are usually manufactured as a package with FC/APC connector where the position of the connector with respect to the lenses is tuned precisely by the manufacturer.[24]

Galvanometric Mirrors: In OCTs, the light spot must be traveled around the cross-section of the sample to achieve 2-D images.[25] To do this, two galvanometric mirrors must be used where each mirror is attached to a dedicated servo motor equipped with a high-precision driver. The servo drivers have the ability of close-loop angle control with microradian precision and fast dynamic response.[26,27]

Objective Lens: Lateral resolution, DOF, and maximum FOV of an OCT depend on the type of the objective lens and its specifications.[28,29] Often, high-quality scan lenses are selected as the objective lens to achieve the desired lateral resolution and FOV. Objective lens is one of the most expensive optical elements used in an OCT.

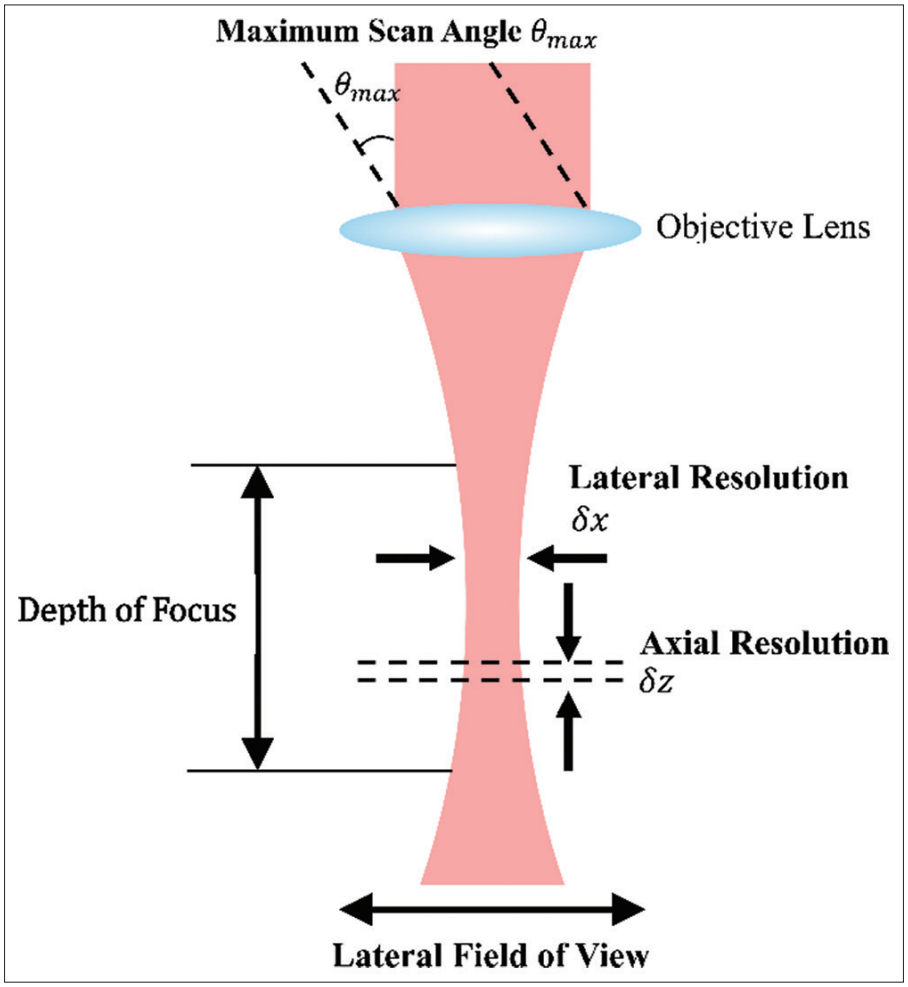

Figure 2: Graphical representation of axial resolution, lateral resolution, depth of focus, and field of view[25]

Reference arm

Optical behavior and length of reference arm must be similar to that of the sample arm. By satisfying this constraint, light rays travel equal lengths in the sample and reference arms; consequently, they return back to the coupler at the same time.[30]

Based on Figure 1, reference arm consists of the following components:

- Collimator
- Dispersion compensator
- Reference mirror.

In the following paragraphs, a brief description is provided about these components.

Collimator: The role of collimator in reference arm is exactly the same as its role in the sample arm; that is, the same collimator used in the sample arm is selected for the reference arm.

Dispersion Compensator: Various divergences occur when the light travels along the objective lens[31] while these diverges are not occurred in the reference arm. Since optical behavior of both the arms must be the same, similar diverges must be applied to the light travels along the reference arm. Therefore, instead of an objective lens, a dispersion compensator is used in the reference arm[32] to generate the required diverges. It must be noted that optical component manufacturers produce a correspondent dispersion compensator for each objective lens which has similar optical divergences with significantly lower cost.

Reference Mirror: A high reflective mirror must be placed at the end of the reference arm so that the light ray hits to this mirror returns back without any variation. To do this, a high-quality mirror with gold or silver coating is used in the reference arm.[33]

Spectrometer arm

Although axial resolution of a SD-OCT depends on central wavelength and bandwidth of the light source, improper design of the spectrometer arm can degrade the axial resolution significantly.[34] Based on Figure 1, spectrometer arm of a SD-OCT consists of the following components:

- Collimator
- Diffraction grating
- Lens network
- Line-scan charge-coupled device (CCD) camera.

In the following paragraphs, a brief description is provided about these components.

Collimator: Role of collimator in the spectrometer arm is exactly the same as its role in the sample arm.

Diffraction grating: Diffraction grating is the key component of spectrometer arm since the light beam entered into the spectrometer is decomposed into its constituent wavelengths through this component.[35] Diffraction gratings are constructed such that when a broadband light beam is radiated to them the beam is diffracted to numerous light rays with different exiting angles where the exiting angle of each ray is in relation to the wavelength of the diffracted ray.[36]

Lens Network: All of the diffracted light rays must be focused on the pixel array of the CCD camera placed in the spectrometer. Since exiting angle of diffracted light rays is different with each other, a special lens network must be placed after the grating to focus each of the diffracted light rays into a unique pixel on the CCD camera pixel array.[37]

CCD Camera: Line-scan CCD camera is placed at the end of spectrometer. Each pixel of a CCD camera has a dedicated capacitor which is charged in accordance with the intensity of the light ray radiated to the pixel;[38,39] that is, by measuring the voltage of each capacitor, the intensity of the corresponding light ray can be identified. Intensity of each ray provides an information about a specific depth into the sample tissue.[40] Consequently, depth profile of the sample, which is referred to a raw A-scan, can be obtained by measuring the voltage of the CCD camera capacitors.

CCD cameras are equipped with a fast analog-to-digital converter which is used to convert the voltage of the capacitors into a digital array.[41] The generated digital array is transferred to a PC through a high-speed data transmission protocol such as Gigabit Ethernet or Camera Link. The transmitted data are received in the PC where the final A-scan of the sample is obtained by applying various digital signal processing algorithms to the received data.

Optical System Design

Light source and its accessories

In SD-OCT, the SLD used as a light source must be chosen based on the desired axial resolution and maximum penetration depth.[42] Axial resolution and maximum penetration depth in an environment with refractive coefficient of n can be calculated through (1) and (2), respectively: [43]

$$\delta z = \frac{2\ln 2}{n\pi}\frac{{\lambda_0}^2}{\Delta\lambda} \quad (1)$$

$$z_{max} = \frac{N{\lambda_0}^2}{4n\Delta\lambda} \quad (2)$$

Where, δz is axial resolution, z_{max} is maximum penetration depth, λ_0 is central wavelength of light source, $\Delta\lambda$ is bandwidth of light source, n is refraction coefficient, and N is the number of CCD camera pixels.

Light source

Light source is the most important element among the optical components of an SD-OCT due to the fact that axial

Table 1: User requirements of the desired ultrahigh-resolution spectral-domain optical coherence tomography

Feature	Value
A-scan rate	≥70 kHz
Axial resolution (retina)	≤3 μm
Lateral resolution (retina)	≤15 μm
Maximum imaging depth	≥1.5 mm
Field of view	≥15 mm × 15 mm

resolution and penetration depth depend on the light source specifications. Moreover, the other optical components must be selected by considering the light source characteristics such as central wavelength, bandwidth, power intensity, and spectral power distribution.[44] In the following paragraphs, a brief explanation is provided about each of these parameters.

Central wavelength: An important issue in the selection of central wavelength is the amount of light that is absorbed by the sample when the light passes through it. The UHR SD-OCT proposed in this article is designed for retinal application.

The light energy absorption in the retinal layers is similar to energy absorption of the water. Based on a study by Leitgeb *et al.,*[45] the amount of absorbed energy in the water becomes so high for wavelengths >1000 nm. Therefore, the central wavelength of the light sources used in retinal applications is adjusted to around 850 nm which is appropriately lower than 1000 nm.

Bandwidth: According to Jorjandi *et al.,*[2] the imaging depth is increased by decreasing the bandwidth of the light source while the axial resolution is decreased in the same condition; that is, a trade-off exists between axial resolution and maximum imaging depth.

Power distribution: SLD light sources with Gaussian power distribution must be used in SD-OCTs; otherwise, the effective bandwidth is decreased which degrades the axial resolution.

Power intensity: According to ANSI standard,[46] to protect the patient's retina against hazardous radiation, the intensity of the radiated light ray must be kept below the maximum permissible value.

Fiber coupler

Fiber coupler is used to transfer a specified percent of the light into the sample and reference arms. Therefore, power ratio of the fiber coupler must be chosen based on the intensity of the light source output and the threshold value specified in ANSI standard. Moreover, the central wavelength and bandwidth of the fiber coupler must be similar to that of the light source.[47]

Polarization controller

To achieve the maximum interference in the fiber coupler, polarity of the light rays returned back from the sample and reference arms must be adjusted properly. Therefore, polarization controllers are placed before the sample and reference arms to adjust the light ray polarity.[48]

Sample arm

Collimator

Lateral resolution of an OCT is equal to spot size of the light ray on the sample tissue where the amount of spot size depends on the diameter of the light ray travels in the sample arm.

Beam diameter in the sample arm is adjusted by the collimator; that is, the collimator must be selected based on the preferred lateral resolution. Moreover, operating wavelength range of the collimator must be equal or greater than that of the light source.[49]

Galvanometric mirrors

Galvanometric mirrors are used in sample arm to move the light spot around the cross-section of the sample. Resolution, angle step response, and maximum scan angle are the important parameters that must be considered in selection of galvanometric mirror.[50]

Resolution: Resolution indicates the precision of galvanometric mirror and its control system in scanning the cross-section of the sample. Often, the resolution of galvanometric mirrors is in the range of several 10 microradians.

Angle step response: Angle step response is in direct relation to dynamic response of the mirrors. Often, angle step response of galvanometric mirrors is in the range of several hundred microseconds.

Maximum scan angle: Maximum scan angle indicates the range that can be scanned by the mirrors.

Objective Lens

Lateral resolution, DOF, and maximum FOV of a SD-OCT depend on the objective lens. Focal length, diameter, operating wavelength range, and FOV are the important parameters that must be considered in selection of the objective lens.

According to Lee *et al.,*[51] lateral resolution and DOF can be calculated as follows:

$$\delta x = 2\sqrt{2ln2}\,\frac{f\lambda}{n\pi d} \tag{3}$$

$$b = \frac{\pi\delta x^2}{\lambda} \tag{4}$$

Where δx is lateral resolution, f is focal length, d is beam diameter, b and is DOF.

According to Nassif *et al.,*[3] and Ikuno and Tano,[4] it can be observed that a trade-off exists between lateral resolution and DOF; that is, DOF is reduced by improving the lateral resolution (reducing the magnitude of δx).

Reference arm

Optical components of the reference arm must be selected in accordance with the sample arm components.

Collimator

A collimator similar to what is used in the sample arm must be used in the reference arm.

Dispersion compensator

This component must be chosen in accordance with the objective lens; that is, after selecting an objective lens, its corresponding dispersion compensation is selected based on the guidance of the objective lens manufacturer.[52]

Reference mirror

Reference mirror is selected with the objective of obtaining the maximum reachable reflectivity. Various types of mirrors with gold or silver coating are accessible with reflectivity coefficients up to 99%.

Spectrometer arm

Collimator

To achieve the proper spot size in the CCD camera pixel array, a larger beam diameter is required in the spectrometer arm in comparison with the beam diameter in the sample and reference arms.[53] It must be noted that, if spot size of the light ray on the pixel array is not adjusted properly, axial resolution is degraded significantly.

Diffraction grating

In the spectrometer arm, a diffraction grating is essential to diffract the light beam into its constituent wavelengths. Diffraction grating must be selected by considering the following parameters: central wavelength, operating bandwidth, number of grooves, diffraction efficiency in the operating bandwidth, and radiation angle.[54] In the following paragraphs, a brief description is provided about these parameters:

Central wavelength and bandwidth: These two parameters must be compatible with the parameters of the selected light source; otherwise, the effective bandwidth of the light source is reduced which leads to degradation of the axial resolution.

Number of grooves: The number of light rays generated by a diffraction grating as well as the exiting angle of each ray depends on the number of the grating grooves.[55] For a 1800 line/mm diffraction grating, 1800 grooves exist in each millimeter.

Efficiency: This parameter indicates the strength of the grating in diffraction of the radiated light beam.

Radiation Angle: To achieve the highest diffraction efficiency, the light beam must be radiated to the grating surface with a specified angle. After radiating the light to the grating, the light beam is decomposed into its constituent wavelengths where the exiting angle of each ray is calculated as follows:

$$\alpha_i = \sin^{-1}\left(\frac{2\lambda_i - \lambda_{0DG}}{2d_{DG}}\right) \tag{5}$$

where is λ_i wavelength of the light ray radiated to the grating, λ_{0DG} is central wavelength of the grating, and d_{DG} is the distance between two consecutive grooves.

Lens network

Lens network must be designed by considering the following two constraints:

1. Each diffracted ray must be focused on a unique pixel
2. Spot size of each light ray on the pixel array must be almost equal to the pixel size.

Based on a study by Davila *et al.,*[56] to satisfy the two constraints, above, the effective focal length of the lens network must be equal to the following equation:

$$f = \frac{pixels\ number * pixel\ size}{2\tan\left(\frac{\alpha_{max} - \alpha_{min}}{2}\right)} \tag{6}$$

Where, α_{max} and α_{min} are the maximum and minimum values of the exiting angles calculated by (5), and f is effective focal length of the lens network.

To achieve the desired focal length, the number of lenses used in the network, focal length and radius of each lens, relative distance of the lenses from each other, and their positioning angles with respect to the diffraction grating surface must be adjusted carefully.

Spot size of each diffracted light ray on the pixel array can be calculated as follows: [57]

$$w_i = 2\sqrt{2ln2}\,\frac{f\lambda_i}{\pi d} \tag{7}$$

Where is spot size of ith diffracted light, f is calculated by (6), d is diameter of the light beam, and λ_i is wavelength of ith diffracted ray.

Charge-coupled device camera

CCD camera is the slowest part of a SD-OCT; hence, A-scan generation rate of a SD-OCT is equal to line-scan rate of the CCD camera.

The following parameters must be considered in selecting the CCD camera: pixel size, number of pixels, line-scan rate, and data transmission protocol.

Number of pixels: According Jorjandi *et al.,*[2] maximum penetration depth of a SD-OCT depends on this parameter.

Pixel size: Spot size of the diffracted light rays must be adjusted based on this parameter.

Line-scan rate: This parameter identifies the A-scan rate of a SD-OCT.

Transmission protocol: Often, Gigabit Ethernet or Camera Link is used as the transmission protocol of CCD cameras where data transmission rate in Camera Link protocol is significantly higher.

Optical Component Selection

Light source and its accessories

According to the user requirements, specifications of the desired UHR SD-OCT that can be used in retinal application are tabulated in Table 1. According to Mahmudi *et al.,*[1] and Table 1, since n is 1.336 for retina, $\frac{\lambda_0^2}{\Delta\lambda}$ must be smaller than 0.6874 to achieve the desired axial resolution. To find a proper light source, the most relevant products of various companies are assessed where the results are summarized in Table 2. As observed, EBS300002-03 light source made by Exalos Inc. is the best choice among the others.

According to risk analysis, intensity of the light ray radiated to the patient's eyes must be kept below the maximum permissible value reported in ANSI standard. To satisfy this constraint, EBS300002-03 is equipped with an internal protection unit that control the output intensity continuously.

Based on the selected light source specifications, TW850R5A2 [Table 3] made by Thorlabs Inc.[58] is selected as the fiber coupler and IO-F-SLD100-840 [Table 4] made by Thorlabs Inc. is selected as the optical isolator.

Sample arm

According to Nassif *et al.,*[3] and user requirements tabulated in Table 1, since n is 1.336 for retina, the value of $\frac{f}{\mathrm{d}}$ must be smaller than 30.901 to achieve the desired lateral resolution. Since is adjusted by the collimator, proper collimator is selected at first.

Collimator

Often, beam diameter in the sample arm of a SD-OCT is adjusted to 1.2–1.8 mm.[48] Hence, F240APC-850 [Table 5] made by Thorlabs Inc. is selected as the collimator.

Objective lens

According to Table 5, beam diameter in the sample arm is 1.74 mm; hence, focal length of the objective lens must be smaller than 54.11 mm to achieve the desired lateral resolution. On the other hand, maximum FOV of a SD-OCT is equal to maximum FOV of the objective lens; that is, FOV of the selected objective lens must be greater than the FOV value presented in Table 1. Therefore, LSM54-850 [Table 6] made by Thorlabs Inc. is selected as the objective lens.

Galvanometric mirrors

According to requirements of the galvanometric mirrors presented in subsection 3.2.2, GVSM002-ECLM [Table 7] made by Thorlabs Inc. is selected as the galvanometric mirror system. GVSM002-ECLM includes two DC servo motors, two galvanometric mirrors, two high-precision position control driver boards, and a low-noise linear power supply. Driver boards can control the mirrors in a closed-loop manner with high precision, negligible steady-state error, fast dynamic response, and ultra-low oscillation and drift.

Reference arm

Collimator

The same collimator used in the sample arm, i.e., F240APC-850, is selected for the reference arm.

Dispersion compensator

LSM54DC1 [Table 8] which is suggested by Thorlabs Inc. to use as the corresponding dispersion compensator of LSM54-850 objective lens is selected for the reference arm.

Reference mirror

Protected gold mirrors are ideal choices for use in infrared wavelength range since they are insensitive to angle of radiation and have very high reflectivity; hence, PF10-03-M01 [Table 9] which is a gold-coated mirror made by Thorlabs Inc. is selected as the reference mirror.

Spectrometer arm

Collimator

Often, the collimator placed in spectrometer arm is selected such that its output beam diameter be larger than that of the sample arm; hence, F260APC-850 [Table 10] made by Thorlabs Inc. is selected as the collimator for the spectrometer arm.

Diffraction grating

According to the requirements presented in subsection 3.4.2, WP-HD1800/840-25.4 holographic grating [Table 11] made by Wasatch Photonics Inc.[62] is selected as diffraction grating for the spectrometer arm. This grating has excellent efficiency, minimum stray light, and negligible polarization dependency.

Based on Srinivasan *et al.,*[5] and Table 11, since λ_i varies between 815 and 915 nm, α_i varies between 45.37 and 63.11°.

Charge-coupled device camera

According to the requirements presented in subsection 3.4.4, EV71YEM4CL2010-BA9 line-scan camera [Table 12] made by E2V Semiconductor Inc.[63] is selected as the CCD camera. This camera is a special version of AVIIVA EM4 line-scan cameras produced for OCT applications.

Based on Zhang *et al.,*[6] and Table 12, the effective focal length of the lens network must be 65.6 mm to achieve the desired axial resolution. However, according to Drexler *et al.*,[7] since λ_i varies between 815 and 915 nm, w_i varies between 12.07 and 13.55 μm which is a bit larger than the pixel size of the selected CCD camera. Consequently, the axial resolution is degraded effectively.

To overcome this problem, effective focal length of the lens network must be reduced to 48.4 mm. By doing so, w_i varies between 8.90 and 10 μm. Consequently, based on Drexler *et al.*,[7] the number of pixels that receipt the light rays is reduced to 1511 pixels which reduces the maximum imaging depth; that is, a trade-off exists between axial resolution and maximum imaging depth. Since axial resolution has the highest priority among the other features, in this study, effective focal length of the lens network is adjusted to 48.4 mm to achieve the best axial resolution. Therefore, based on Jorjandi *et al.*,[2] and Table 12, the maximum imaging depth is 2.115 mm.

As mentioned earlier, A-scan rate of SD-OCT is equal to line-scan rate of the selected CCD camera. As a result, based on Table 12, A-scan rate of the designed UHR SD-OCT is 70 kHz.

Lens network

Lens network must be designed such that all diffracted rays be focused on the CCD camera pixel array. To satisfy this constraint, lens network must be designed by considering the selected CCD camera parameters [Table 12] as well as the preferred focal length and spot size identified in subsection 4.4.3.

To find the best lens network, various optical systems are simulated in ZIMAX software. After investigating the simulation results and comparing the performance of the networks with the desired performance, the lens network illustrated in Figure 3 is selected as the best choice. As can be observed, two unmounted achromatic doublet lenses with the part number of AC254-040-B [Table 13] are placed back-to-back to realize a lens network[58] while the location and angle of the lenses with respect to the grating surface are adjusted according to Table 14.

Simulation Results

To assess the effectiveness of the selected optical isolator to avoid light rays to travel back to the light source, a simulation is conducted in ZIMAX software where the results are shown in Figure 4. As observed, the intensity of the light ray traveled back to the light source is almost negligible.

To assess the effectiveness of the proposed reference arm, various simulations are conducted in ZIMAX software where intensity of the reflected light ray with respect to intensity of the light entered to the reference arm is calculated and demonstrated in Figure 5. As observed, the selected gold mirror has an acceptable reflectivity while the selected dispersion compensator has negligible effect on the intensity of the reflected light ray.

As mentioned earlier, lateral resolution of a SD-OCT is related to the sample arm optical components. To assess the effectiveness of the selected galvanometric mirrors as well as the selected objective lens to achieve the desired lateral resolution, various simulations are conducted in ZIMAX software where the results are presented in Figure 6. As can be observed, the spot size of the light ray on the whole cross-section of the sample is below the minimum lateral resolution required in the desired UHR SD-OCT device.

To assess the effectiveness of the proposed spectrometer arm, various simulations are conducted in ZIMAX software where the results are presented in this section. In these simulations, the lens network is modeled as shown in Figure 3.

As mentioned earlier, lens network is designed such that the following goals can be obtained: (1) each diffracted ray is radiated on only one pixel, (2) spot size of the rays on the CCD camera array be smaller than the pixel size, and (3) all diffracted rays be focused on the CCD camera array.

To assess whether the proposed lens network can meet the constraint, above, a simulation is conducted in Zemax software where the location and spot size of some of the diffracted rays on the CCD camera pixel array are presented in Figures 4 and 5. As observed, each ray is only focused on one pixel [Figure 7] while the spot size of the diffracted ray is smaller than the CCD camera pixel size [Figure 8].

Since spot size of diffracted light rays depends on wavelength of the diffracted ray,[64] spot size variations with respect to wavelength of the diffracted light rays are plotted in Figure 9. According to this figure, spot size of all diffracted light rays is sufficiently smaller than the CCD camera pixel size.

To assess the performance of the proposed spectrometer arm in constructing a real image from the sample, the proposed

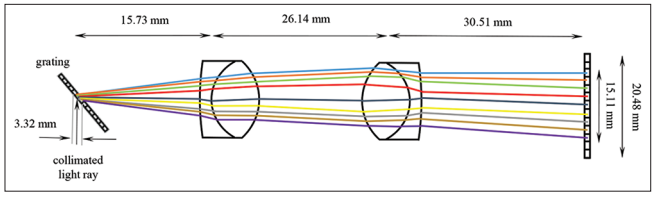

Figure 3: The designed lens network

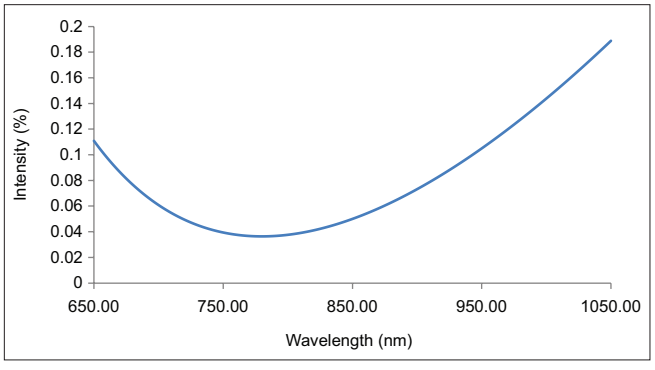

Figure 4: Intensity of the light traveled back to the light source with respect to the intensity of the produced light ray

spectrometer is simulated as an optical system where its optical aberration is assessed through Zemax software. The simulation results are presented in Figures 10-13.

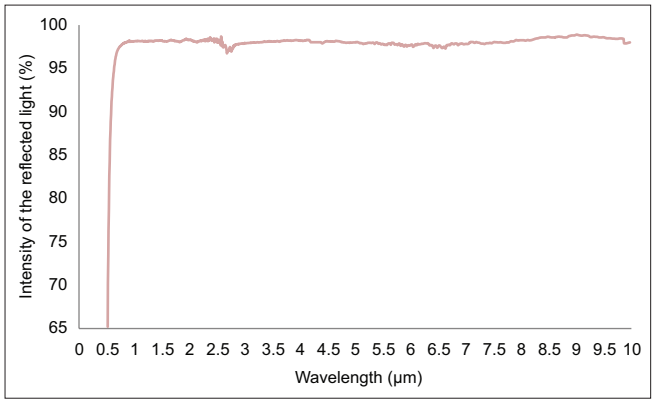

Figure 5: Intensity of the reflected light ray with respect to the intensity of the light entered into the reference arm

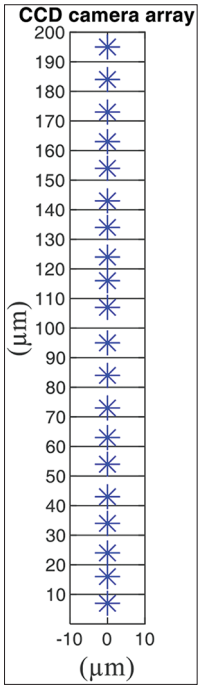

Figure 7: Simulation result: location of the light rays focused on the charge-coupled device camera array. CCD: Charge-coupled device

According to Figure 10, distance of the sagittal rays from chief ray is smaller than ± 10 μm while distance of the tangential rays from chief ray is smaller than ± 7 μm. This means that in the proposed spectrometer arm, all the diffracted light rays are focused on the CCD camera pixels without any significant distortion.

According to Figure 11, optical pass difference in the proposed spectrometer is smaller than ± 0.1 μm for both the sagittal and tangential rays which means that

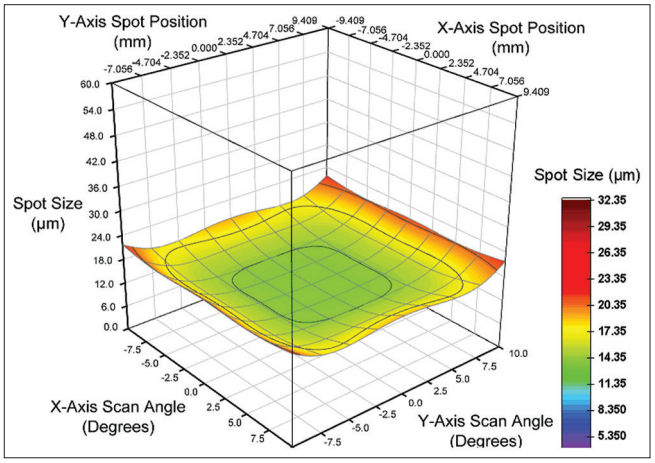

Figure 6: Spot size of the light ray penetrated into the sample tissue for various scan angles

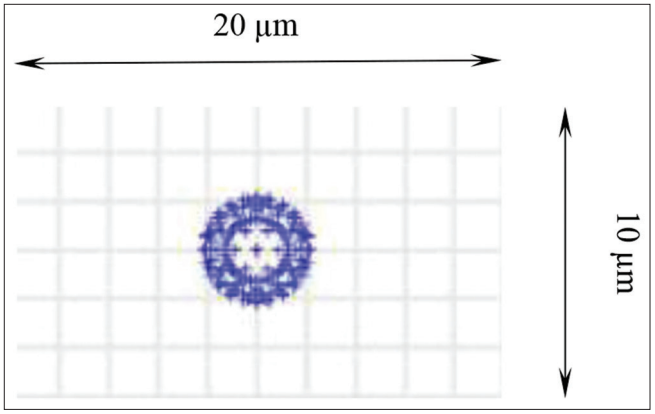

Figure 8: Simulation result: spot size of a light ray with wavelength of 850 nm on a charge-coupled device camera

Table 2: Light sources and their axial resolution

Part number	Company	Laser type	λ_0 (μm)	$\Delta\lambda$ (μm)	Δz (retina) (μm)	Power (mW)
SLD850S-A10W	Thorlabs[58]	SLD	850	60	3.997	10
SLD880-A7	Thorlabs[58]	SLD	880	40	6.394	7
OESLD830-50	O-E Land[59]	SLD	830	50	4.550	1
OESLD920-30	O-E Land[59]	SLD	920	30	9.318	1
QSDM-880-2	QPhotonics[60]	SLD	880	20	12.789	2
QSDM-915-2	Qphotonics[60]	SLD	915	45	6.145	2
EBS300002-03	Exalos[61]	SLD	865	100	2.353	9
EBS300080-02	Exalos[61]	SLD	845	140	1.684	9

SLD: Super luminescent diode

the diffracted light rays are focused with negligible distortion.

According to Figure 12, field angle in the worst case is about 5° while longitudinal shift from the central wavelength is smaller than ± 60 μm for all diffracted light rays. This means that the proposed spectrometer has the ability of focusing all the diffracted light rays on the CCD camera array with proper spot size and optical specification.

According to Figure 13, root mean square wavefront error for all diffracted light rays is smaller than 0.025

Table 3: TW850R5A2 coupler specifications

Feature*	Value*
Central wavelength	850 nm
Bandwidth	±100 nm
Coupling ratio	50:50

*Parameters are presented from[58]

Table 4: IO-F-SLD100-840 isolator specifications

Feature*	Value*
Central wavelength	840 nm
Bandwidth	100 nm
Transmission	66%–69%
Attenuation	23.5%–26%
Connector	FC/APC

*Parameters are presented from[58]

Table 5: F240APC-850 collimator specifications

Feature*	Value*
Center wavelength	850 nm
Wavelength range	650~1050 nm
Output beam diameter	1.74 mm
Focal length	8.02 mm
Full-angle divergence	<0.11°
Connector	FC/APC

*Parameters are presented from[58]

Table 6: LSM54-850 objective lens specifications

Feature*	Value*
Center wavelength	850 nm
Bandwidth	±100 nm
Focal length	54 mm
Field of view	15.8 mm × 15.8 mm

*Parameters are presented from[58]

Table 7: GVSM002-ECLM specifications

Feature*	Value*
Material	Quartz
Coating	Protected silver
Wavelength range	500~2000 nm
Linearity	99.9%
Resolution	15 μrad
Maximum scan angle	±12.5°
Peak current	5 A
Small angle (±0.2°) bandwidth	0–1000 Hz
Small angle step response	300 μs

*Parameters are presented from[58]

Table 8: LSM54DC1 dispersion compensator specifications

Feature*	Value*
Material	N-F2
Coating range	750~950 nm
Glass thickness	37.2 mm
Compatible lens	LSM54-850

*Parameters are presented in[58]

Table 9: PF10-03-M01 mirror specifications

Feature*	Value*
Diameter	25.4 mm
Thickness	6 mm
Wavelength range	800~2000 nm
Reflectance	>96%
Substrate	Fused silica

*Parameters are presented from[58]

Table 10: F260APC-850 collimator specifications

Feature*	Value*
Center wavelength	850 nm
Wavelength range	650~1050 nm
Output beam diameter	3.32 mm
Focal length	15.33 mm
Full-angle divergence	<0.11°
Connector	FC/APC

*Parameters are presented from[58]

Table 11: WP-HD1800/840-25.4 grating specifications

Feature*	Value*
Center wavelength	840 nm
Thickness	3 mm
Diameter	25.4 mm
Angle of incidence	49.1°
Spatial frequency	1800 lines/mm
Substrate	1.5 mm BK7

*Parameters are presented from[62]

Table 12: EV71YEM4CL2010-BA9 camera specifications

Feature*	Value*
Pixels number	2048
Pixels size	10 μm × 20 μm
Line-scan rate	70 kHz
Output data rate	16 Mbits/s
Output interface	Camera link® base/medium
Power	12–24 V, 2 A

*Parameters are presented from[63]

Table 13: AC254-040-B specifications

Feature*	Value*
Diameter	25.4 mm
Focal length	40 mm
Center wavelength	840 nm
Wavelength range	650~1050 nm

*Parameters are presented from[58]

Table 14: Parameters of the designed lens network

Parameter	Value
Distance between grating and lens number 1	15.73 mm
Distance between lens number 1 and lens number 2	26.14 mm
Distance between lens number 2 and CCD camera	30.51 mm
Lens number 1 angle with respect to grating	40.9°
Lens number 2 angle with respect to grating	40.9°

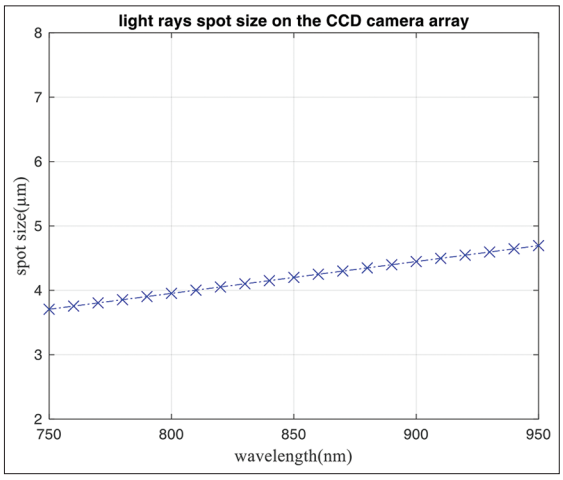

Figure 9: Spot size of all diffracted light rays. CCD: Charge-coupled device

which means that the real wavefront of the proposed optical system is significantly align with the desired wavefront.

Conclusions and Future Works

In this article, a UHR SD-OCT is designed for high-resolution retinal applications. SD-OCT designing is a challenging procedure since various trade-offs exist between SD-OCT features such as axial resolution, maximum penetration depth, lateral resolution, and DOF; hence, optical component selection must be conducted by considering the features with the highest priorities.

Based on the design procedure introduced in this article, although the key features of a UHR SD-OCT depend on the characteristics of the light source and objective lens, improper design of the spectrometer arm can diverge the diffracted light rays and radiate them to wrong locations; that is, in spite of proper design of the sample and reference arms, improper design of the spectrometer arm can defect axial resolution, lateral resolution, etc., significantly.

Lens network configuration is another challenging procedure in designing the UHR SD-OCT. In this procedure, the lens network must be designed such that all diffracted light rays be focused on proper location. Often, various simulations must be conducted for fine-tuning the lens network parameters.

The design procedure of an UHR SD-OCT is presented in detail in this article; however, implementation of this optical system which is a complex and time-consuming

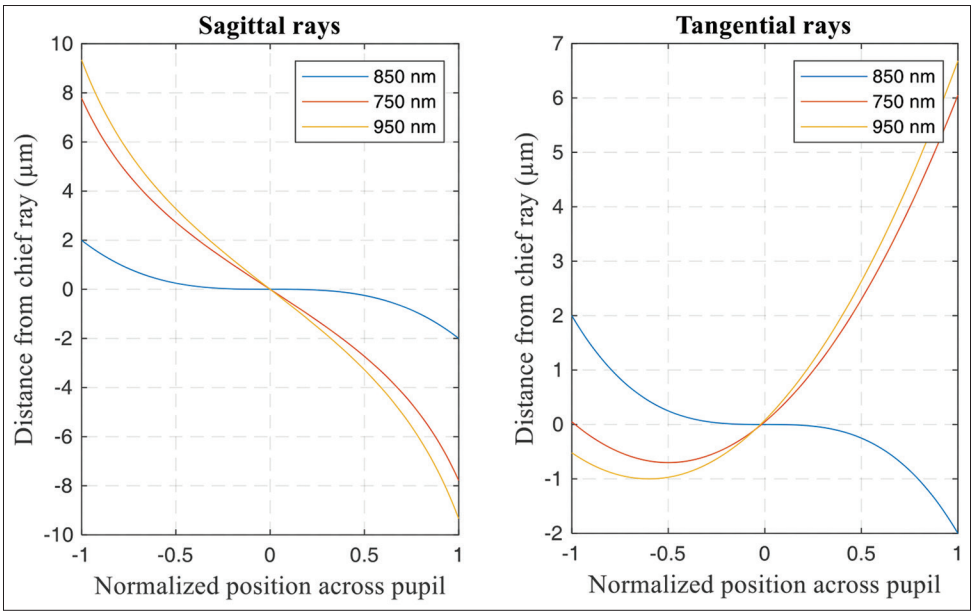

Figure 10: Distance from chief ray versus normalized position across pupil for diffracted light rays

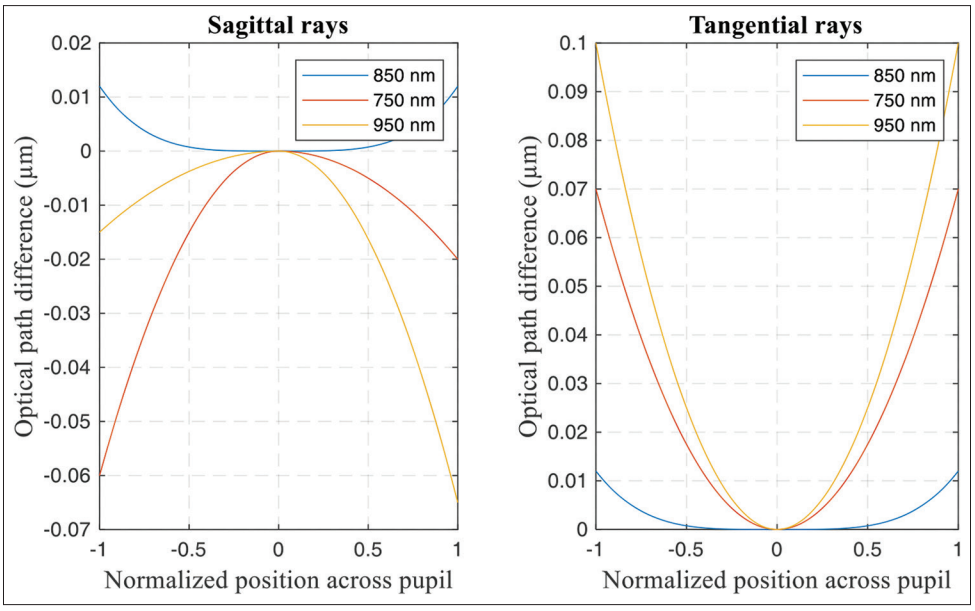

Figure 11: Optical pass difference versus normalized position across pupil for diffracted light rays

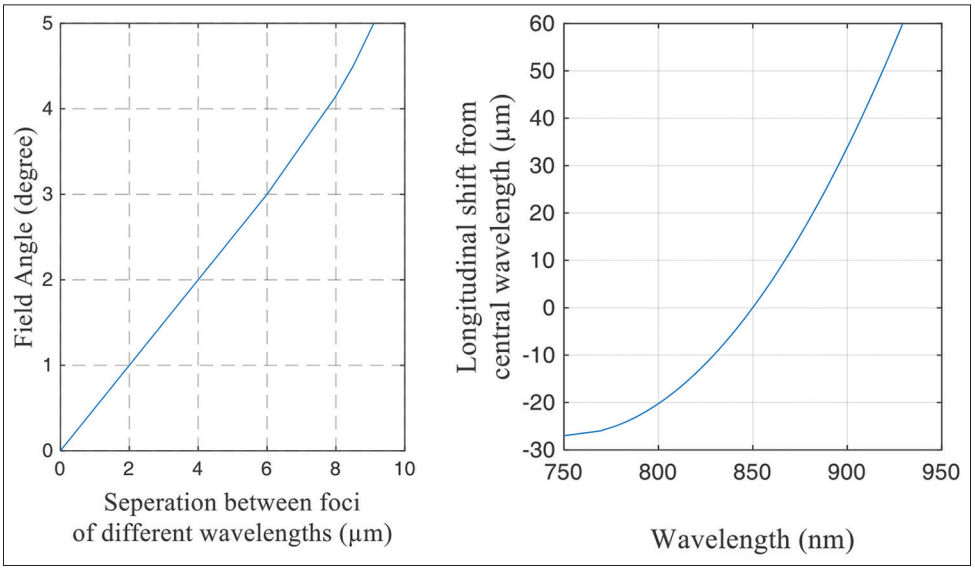

Figure 12: Longitudinal shift from central wavelength

procedure is under research as a future work. An expert laboratory equipped with high-performance optical equipment is required to implement the proposed device and conduct various examinations. After implementing the proposed UHR SD-OCT, various supplementary examinations can be conducted to further assess the performance of the proposed device, for example, different patterns can be employed to scan the cross-section of the sample; then, the effects of each pattern on the A-scan rate, axial resolution, and lateral resolution of the UHR SD-OCT can be investigated. In addition, after obtaining raw A-scans from the constructed device, various digital signal processing algorithms including traditional algorithms, neural network-based algorithms, and deep learning-based algorithms can be adopted to extract 2-D and 3-D images; then, the effectiveness of each algorithm on the quality of the extracted images can be investigated. Moreover, various len networks can be employed in the spectrometer arm to assess the effects of each network on the axial resolution and maximum penetration depth of the proposed UHR SD-OCT.

Acknowledgement and Financial Support

This work was supported in part by the Vice-Chancellery for Research and Technology, Isfahan University of Medical Sciences, under Grant 2403143 and Grant 198095; and in part by the National Institute for Medical Research Development (NIMAD) under Grant 976795.

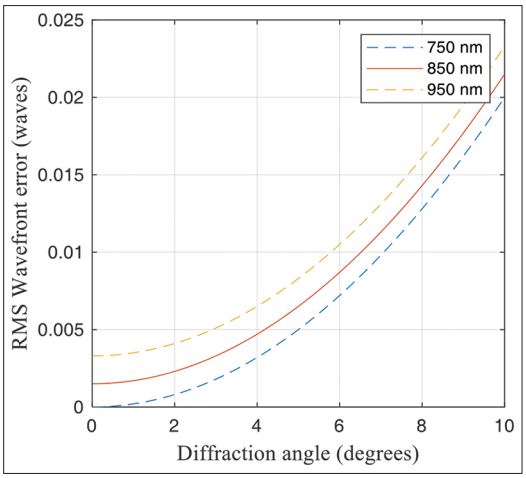

Figure 13: Root mean square wavefront error versus diffraction angle for diffracted light rays. RMS: Root mean square

Conflicts of interest

There are no conflicts of interest.

References

1. Mahmudi T, Kafieh R, Rabbani H, Mehri A, Akhlaghi MR. Evaluation of asymmetry in right and left eyes of normal individuals using extracted features from optical coherence tomography and fundus images. J Med Signals Sens 2021;11:12-23.
2. Jorjandi S, Amini Z, Rabbani H. Super-resolution of retinal optical coherence tomography images using statistical modeling. J Med Signals Sens 2024;14:2.
3. Nassif N, Cense B, Park B, Pierce M, Yun S, Bouma B, *et al. In vivo* high-resolution video-rate spectral-domain optical coherence tomography of the human retina and optic nerve. Opt Express 2004;12:367-76.
4. Ikuno Y, Tano Y. Retinal and choroidal biometry in highly myopic eyes with spectral-domain optical coherence tomography. Invest Ophthalmol Vis Sci 2009;50:3876-80.
5. Srinivasan VJ, Chen Y, Duker JS, Fujimoto JG. *In vivo* functional imaging of intrinsic scattering changes in the human retina with high-speed ultrahigh resolution OCT. Opt Express 2009;17:3861-77.
6. Zhang Q, Lu R, Wang B, Messinger JD, Curcio CA, Yao X. Functional optical coherence tomography enables *in vivo* physiological assessment of retinal rod and cone photoreceptors. Sci Rep 2015;5:9595.
7. Drexler W, Liu M, Kumar A, Kamali T, Unterhuber A, Leitgeb RA. Optical coherence tomography today: Speed, contrast, and multimodality. J Biomed Opt 2014;19:071412.
8. Wojtkowski M, Srinivasan V, Fujimoto JG, Ko T, Schuman JS, Kowalczyk A, *et al.* Three-dimensional retinal imaging with high-speed ultrahigh-resolution optical coherence tomography. Ophthalmology 2005;112:1734-46.
9. Eghtedar RA, Esmaeili M, Peyman A, Akhlaghi M, Rasta SH. Automatic choroidal segmentation in optical coherence tomography images based on curvelet transform and graph theory. J Med Signals Sens 2023;13:92-100.
10. Esmaeili M, Dehnavi AM, Rabbani H, Hajizadeh F. Speckle noise reduction in optical coherence tomography using two-dimensional curvelet-based dictionary learning. J Med Signals Sens 2017;7:86-91.
11. Choma M, Sarunic M, Yang C, Izatt J. Sensitivity advantage of swept source and Fourier domain optical coherence tomography. Opt Express 2003;11:2183-9.
12. Leitgeb R, Hitzenberger C, Fercher A. Performance of Fourier domain versus. time domain optical coherence tomography. Opt Express 2003;11:889-94.
13. Spaide RF, Akiba M, Ohno-Matsui K. Evaluation of peripapillary intrachoroidal cavitation with swept source and enhanced depth imaging optical coherence tomography. Retina 2012;32:1037-44.
14. Chinn SR, Swanson EA, Fujimoto JG. Optical coherence tomography using a frequency-tunable optical source. Opt Lett 1997;22:340-2.
15. Adhi M, Duker JS. Optical coherence tomography – Current and future applications. Curr Opin Ophthalmol 2013;24:213-21.
16. Ishida S, Nishizawa N, Ohta T, Itoh K. Ultra-high resolution optical coherence tomography in 1.7 m region with fiber laser supercontinuum in low-water-absorption samples. Appl Phys Express 2011;4:052501.
17. Braaf B, Vermeer KA, de Groot M, Vienola KV, de Boer JF. Fiber-based polarization-sensitive OCT of the human retina with correction of system polarization distortions. Biomed Opt Express 2014;5:2736-58.
18. An L, Li P, Lan G, Malchow D, Wang RK. High-resolution 1050 nm spectral domain retinal optical coherence tomography at 120 kHz A-scan rate with 6.1 mm imaging depth. Biomed Opt Express 2013;4:245-59.
19. Li P, An L, Lan G, Johnstone M, Malchow D, Wang RK. Extended imaging depth to 12 mm for 1050-nm spectral domain optical coherence tomography for imaging the whole anterior segment of the human eye at 120-kHz A-scan rate. J Biomed Opt 2013;18:16012.
20. Yang V, Gordon M, Qi B, Pekar J, Lo S, Seng-Yue E, *et al.* High speed, wide velocity dynamic range Doppler optical coherence tomography (Part I): System design, signal processing, and performance. Opt Express 2003;11:794-809.
21. Atry F, Pashaie R. Analysis of intermediary scan-lens and tube-lens mechanisms for optical coherence tomography. Appl Opt 2016;55:646-53.
22. Kim J, Brown W, Maher JR, Levinson H, Wax A. Functional optical coherence tomography: Principles and progress. Phys Med Biol 2015;60:R211-37.
23. Srinivasan VJ, Adler DC, Chen Y, Gorczynska I, Huber R, Duker JS, *et al.* Ultrahigh-speed optical coherence tomography for three-dimensional and en face imaging of the retina and optic nerve head. Invest Ophthalmol Vis Sci 2008;49:5103-10.
24. Hafez M, Sidler T, Salathe R. Study of the beam path distortion profles generated by a two-axis tilt single-mirror laser scanner. Opt Eng 2003;42:1048-57.
25. Zhang A, Zhang Q, Chen CL, Wang RK. Methods and algorithms for optical coherence tomography-based angiography: A review and comparison. J Biomed Opt 2015;20:100901.
26. Kennedy BF, Kennedy KM, Sampson DD. A review of optical coherence elastography: Fundamentals, techniques and prospects. IEEE J Sel Top Quantum Electron 2014;20:272-88.
27. Dorrer C, Belabas N, Likforman JP, Jofre M. Spectral resolution and sampling issues in fourier-transform spectral interferometry. J Opt Soc Am B Opt Phys 2000;17:1795-802.
28. Bille J. High Resolution Imaging in Microscopy and Ophthalmology. New Frontiers in Biomedical Optics. 1st ed. Switzerland: Springer; 2019.
29. Kou L, Labrie D, Chylek P. Refractive indices of water and ice in the 0.65- to 2.5-microm spectral range. Appl Opt 1993;32:3531-40.

30. Chong SP, Merkle CW, Cooke DF, Zhang T, Radhakrishnan H, Krubitzer L, *et al.* Noninvasive, *in vivo* imaging of subcortical mouse brain regions with 1.7 μm optical coherence tomography. Opt Express 2015;40:4911-4. doi: 10.1364/OL.40.004911.
31. Fernández E, Hermann B, Považay B, Unterhuber A, Sattmann H, Hofer B, *et al.* Ultra-high resolution optical coherence tomography and pancorrection for cellular imaging of the living human retina. Opt Express 2008;16:11083-94.
32. Hattori Y, Kawagoe H, Ando Y, Yamanaka M, Nishizawa N. High-speed ultrahigh-resolution spectral domain optical coherence tomography using high-power supercontinuum at 0.8 μm wavelength. Appl Phys Express 2015;8:082501.
33. de Boer JF, Cense B, Park BH, Pierce MC, Tearney GJ, Bouma BE. Improved signal-to-noise ratio in spectral-domain compared with time-domain optical coherence tomography. Opt Lett 2003;28:2067-9.
34. Zawadzki RJ, Jones SM, Pilli S, Balderas-Mata S, Kim DY, Olivier SS, *et al.* Integrated adaptive optics optical coherence tomography and adaptive optics scanning laser ophthalmoscope system for simultaneous cellular resolution *in vivo* retinal imaging. Biomed Opt Express 2011;2:1674-86.
35. Zawadzki RJ, Jones SM, Olivier SS, Zhao M, Bower BA, Izatt JA, *et al.* Adaptive-optics optical coherence tomography for high-resolution and high-speed 3D retinal *in vivo* imaging. Opt Express 2005;13:8532-46.
36. Unterhuber A, Povazay B, Hermann B, Sattmann H, Chavez-Pirson A, Drexler W. *In vivo* retinal optical coherence tomography at 1040 nm – Enhanced penetration into the choroid. Opt Express 2005;13:3252-8.
37. Povazay B, Bizheva K, Hermann B, Unterhuber A, Sattmann H, Fercher A, *et al.* Enhanced visualization of choroidal vessels using ultrahigh resolution ophthalmic OCT at 1050 nm. Opt Express 2003;11:1980-6.
38. Froehly L, Ouadour M, Furfaro L, Sandoz P, Leproux P, Huss G, *et al.* Spectroscopic OCT by grating-based temporal correlation coupled to optical spectral analysis. Int J Biomed Imaging 2008;2008:752340.
39. Ichikawa H, Yasuno Y, Fujibuchi H. Optical coherence tomography interpreted by diffractive optics: A-scan image formation with wavelength-scale diffraction gratings as samples. OSA Contin 2020;3:2395-406.
40. Barrick J, Doblas A, Gardner MR, Sears PR, Ostrowski LE, Oldenburg AL. High-speed and high-sensitivity parallel spectral-domain optical coherence tomography using a supercontinuum light source. Opt Lett 2016;41:5620-3.
41. Ishida S, Nishizawa N. Quantitative comparison of contrast and imaging depth of ultrahigh-resolution optical coherence tomography images in 800-1700 nm wavelength region. Biomed Opt Express 2012;3:282-94.
42. Park B, Pierce MC, Cense B, Yun SH, Mujat M, Tearney G, *et al.* Real-time fiber-based multi-functional spectral-domain optical coherence tomography at 1.3 microm. Opt Express 2005;13:3931-44.
43. Nakamura Y, Makita S, Yamanari M, Itoh M, Yatagai T, Yasuno Y. High-speed three-dimensional human retinal imaging by line-field spectral domain optical coherence tomography. Opt Express 2007;15:7103-16.
44. Atry F, Rosa IJ, Rarick KR, Pashaie R. Design and implementation guidelines for a modular spectral-domain optical coherence tomography scanner. Int J Opt 2018. p. 1-22.
45. Leitgeb RA, Villiger M, Bachmann AH, Steinmann L, Lasser T. Extended focus depth for Fourier domain optical coherence microscopy. Opt Lett 2006;31:2450-2.
46. Dhalla AH, Migacz JV, Izatt JA. Crosstalk rejection in parallel optical coherence tomography using spatially incoherent illumination with partially coherent sources. Opt Lett 2010;35:2305-7.
47. Gelikonov VM, Gelikonov GV, Shilyagin PA. Linear wave number spectrometer for high-speed spectral-domain optical coherence tomography. Opt Spectrosc 2009;106:459-65.
48. Tomlins PH, Wang RK. Theory, developments and applications of optical coherence tomography. J Phys D Appl Phys 2005;38:2519-35.
49. Kowalevicz A, Ko T, Hartl I, Fujimoto J, Pollnau M, Salathé R. Ultrahigh resolution optical coherence tomography using a superluminescent light source. Opt Express 2002;10:349-53.
50. Lee SW, Jeong HW, Kim BM, Ahn YC, Jung W, Chen Z. Optimization for axial resolution, depth range, and sensitivity of spectral domain optical coherence tomography at 1.3 μm. J Korean Phys Soc 2009;55:2354-60.
51. Lee B, Chen S, Moult EM, Yu Y, Alibhai AY, Mehta N, *et al.* High-speed, ultrahigh-resolution spectral-domain OCT with extended imaging range using reference arm length matching. Transl Vis Sci Technol 2020;9:12.
52. Fathipour V, Bonakdar A, Mohseni H. Advances on sensitive electron-injection based cameras for low-flux, short-wave infrared applications. Front Mater 2016;3:1-16.
53. Al-Qazwini Z, Ko ZY, Mehta K, Chen N. Ultrahigh-speed line-scan SD-OCT for four-dimensional *in vivo* imaging of small animal models. Biomed Opt Express 2018;9:1216-28.
54. Hyeon MG, Kim HJ, Kim BM, Eom TJ. Spectral domain optical coherence tomography with balanced detection using single line-scan camera and optical delay line. Opt Express 2015;23:23079-91.
55. Chan KK, Tang S. High-speed spectral domain optical coherence tomography using non-uniform fast Fourier transform. Biomed Opt Express 2010;1:1309-19.
56. Davila A, Huntley JM, Pallikarakis C, Ruiz PD, Coupland JM. Wavelength scanning interferometry using a Ti: Sapphire laser with wide tuning range. Opt Lasers Eng 2012;50:1089-96.
57. Kalkman J. Fourier-domain optical coherence tomography signal analysis and numerical modeling. Int J Opt 2017. p. 16.
58. Available from: https://www.thorlabs.com/. [Last accessed on 2024 Feb 24].
59. Available from: https://www.o-eland.com/. [Last accessed on 2024 Feb 24].
60. Available from: https://www.qphotonics.com/. [Last accessed on 2024 Feb 24].
61. Available from: https://www.exalos.com/. [Last accessed on 2024 Feb 24].
62. Available from: https://wasatchphotonics.com/. [Last accessed on 2024 Feb 24].
63. Available from: https://www.teledyne.com/. [Last accessed on 2024 Feb 24].
64. Izatt JA, Choma MA. Theory of optical coherence tomography. In: Optical Coherence Tomography: Technology and Applications. Switzerland: Springer; 2008. p. 47-72.